

P. A. Raynaud,¹ D. A. Koss,¹ A. T. Motta,² and K. S. Chan³

Fracture Toughness of Hydrided Zircaloy-4 Sheet Under Through-Thickness Crack Growth Conditions

ABSTRACT: The susceptibility of fuel cladding to failure in the case of a postulated reactivity-initiated accident may be determined by crack initiation within a hydride blister or rim and subsequent crack growth through the thickness of the cladding. This study has determined the fracture toughness of hydrided cold-worked stress relieved Zircaloy-4 sheet subject to *through-thickness* crack growth at both 25 and 300°C. The experimental approach utilizes a novel procedure in which a narrow linear strip of brittle hydride blister across the specimen width creates a well-defined precrack upon initial loading. The subsequent crack growth resistance is then characterized by four-point bending of the specimen and an elastic-plastic fracture mechanics analysis. At room temperature, the through-thickness fracture toughness (K_{Ic}) is sensitive to the orientation of the hydride platelets and $K_{Ic} \approx 25 \text{ MPa}\sqrt{\text{m}}$ for crack growth through a mixed in-plane/out-of-plane hydride field. In contrast, K_{Ic} is much higher ($\approx 75 \text{ MPa}\sqrt{\text{m}}$) when the hydride platelets are oriented predominantly in the plane of the sheet and therefore normal to both the crack plane and the crack growth direction. At 300°C, the material exhibits greater ductility as the hydride particles within the matrix resist fracture such that $K_{Ic} \approx 83 \text{ MPa}\sqrt{\text{m}}$, despite the much lower flow stress of the material.

KEYWORDS: Zircaloy, hydrides, fracture toughness

Introduction

During reactor exposure, the ductility of thin-wall zirconium components such as fuel cladding can be degraded by hydrogen ingress associated with waterside corrosion. The resulting uptake of hydrogen has long been identified as a main contributor to limiting the fracture resistance of cladding even at high burnup levels [1,2]. In particular, the cladding ductility is known to be sensitive not only to its total hydrogen content but also to the hydride distribution and orientation (i.e., solid hydride blister, sunburst, radial, or circumferential hydride particles). For thin-wall components such as cladding, the most severe form of hydrogen-induced loss of ductility occurs when a surface crack initiates within a hydride rim or blister and subsequently propagates in a *through-thickness crack-growth mode* [3–6]. In order to predict the cladding performance/ductility under such a “worst-case” condition under quasi-static loading, it is essential to know the following: (a) the initial crack depth, (b) the relevant hydride microstructure through which the crack grows (i.e., radial versus circumferential hydrides), (c) the appropriate temperature (or range of temperatures), (d) the stress state under which deformation occurs, and importantly (e) the fracture toughness under through-thickness crack growth conditions for the appropriate temperature and hydride microstructure.

The fracture toughness for through-thickness crack growth of a thin-wall Zircaloy cladding in the hydrided condition is yet to be determined. In fact, we are aware of no such determination in any thin sheet metal. It is important to recognize that crack growth through the cladding wall thickness occurs under both stress-state *and* hydride microstructure conditions that are distinctly different from other fracture toughness specimen geometries. For example, when the fracture toughness of hydrided zirconium alloys is determined for the case of Mode I crack growth of plate material [7–12], plane-strain is typically imposed along much of the crack front, resulting in a locally high degree of stress triaxiality within the crack-tip plastic zone. Alternatively, while fracture toughness has been determined for hydrided Zircaloy cladding tubes,

Manuscript received April 16, 2007; accepted for publication November 5, 2007; published online December 2007. Presented at ASTM Symposium on Zirconium in the Nuclear Industry: 15th International Symposium on 24–28 June 2007 in Sunriver, OR; Magnus Limback and Bruce Kammenzind, Guest Editors.

¹ Department of Materials Science and Engineering, The Pennsylvania State University, University Park, PA 16802.

² Department of Mechanical and Nuclear Engineering, The Pennsylvania State University, University Park, PA 16802.

³ Southwest Research Institute, San Antonio, TX 78228.

TABLE 1—A comparison of Kearns factors for the present CWSR Zircaloy-4 sheet material with those of Zircaloy-4 cladding tube.

	Normal/Radial	Transverse/Circumferential	Rolling/Axial
CWSR sheet	0.57	0.34	0.16
CWSR tube [4]	0.58	0.32	0.10

crack growth was along the tube axis under a plane stress condition at the crack tip in mixed Mode I/III crack propagation [13]. In contrast, crack growth through the thickness of a cladding tube will very likely occur under a plane-strain condition along the crack front and probably accompanied by a small degree of plastic constraint through the wall thickness; either Mode I or mixed Mode I/II crack growth are likely. The accompanying crack-tip plasticity and damage accumulation process that dictate crack growth will likely differ from those in conventional fracture toughness tests, giving rise to unique fracture toughness values.

In addition, many researchers [8,9,12] have recognized that fracture toughness is sensitive to the morphology and orientation of the hydride platelets with respect to both the crack plane and crack growth direction. Thus, the fracture toughness under a through-thickness crack growth condition in textured *and* hydrided zirconium alloy also creates a crack plane/crack growth direction condition which differs from those of previous fracture toughness studies. For example, hydride platelets aligned in the plane of sheet material (akin to circumferential hydrides in cladding tubes) will be oriented normal to both the crack plane *and* the crack growth direction during through-thickness crack growth. In contrast, out-of-plane hydrides (such as radial hydrides in cladding tubes) would align with both the crack plane and crack growth direction during through-thickness crack growth. Much different fracture toughness values would be expected between these two hydride conditions.

The purpose of this study is to determine the fracture toughness of unirradiated but hydrided cold-worked and stress-relieved (CWSR) Zircaloy-4 subject to *through-thickness* crack growth at both 25 and 300°C *and* as a function of hydride microstructure. With attention to the crack-tip failure processes, the study also seeks to identify the micro-mechanisms that control crack growth resistance and their sensitivity to both temperature and hydride microstructure. Cold-worked and stress-relieved Zircaloy-4 sheet is used as a model material to simulate fracture behavior of thin-wall cladding tube. The study employs a novel experimental procedure to determine the fracture toughness under through-thickness crack growth conditions. The results of this study should be relevant to the development of codes designed to predict the mechanical performance of hydrided thin-wall reactor components under crack-limiting conditions.

Experimental Procedure

Materials

The material used in this study is Zircaloy-4 sheet, 675- μm thick, obtained from Teledyne Wah-Chang initially in the cold-worked (CW) state, and with a composition (in wt. %) of Zr-1.28Sn-0.22Fe-0.12Cr-0.11O. The specimens were subsequently annealed in a vacuum furnace at 10^{-6} Torr and 520°C for two hours in order to obtain a cold-worked stress-relieved (CWSR) material state; no recrystallization was observed. The Kearns texture parameters [14] were subsequently determined using the inverse pole figure method. Table 1 shows that the Kearns parameters are similar to those previously reported for Zircaloy-4 cladding tube [15,16] in the three orthogonal directions.

Tensile testing was also performed in order to characterize the flow behavior of the sheet material. As shown in Table 2, the yield strengths and plastic anisotropy parameter in the transverse direction of the sheet are similar to those of cladding tube material at 25 and 300°C. However, the strain-hardening exponent is significantly smaller for this sheet material. In fact, the strain hardening behavior of this sheet material is similar to that of irradiated cladding [16].

Hydrogen Charging

To determine the fracture toughness, a novel experimental procedure was developed in which a narrow 200–700- μm wide linear strip of hydride blister is created across the width of Zircaloy-4 sheet specimen

TABLE 2—Tensile properties of either CWSR Zircaloy-4 sheet oriented transverse to the rolling direction or Zircaloy-4 cladding tube oriented transverse to its axis.

Temp.	Material	Yield Strength 0.2 % (MPa)	Anisotropy Factor R'	Strain- hardening Exponent n	Elongation to Failure (%)
25°C	CWSR Sheet	575	2.6	0.018	17
	CWSR Cladding [5]	590	2.3	0.068	
300°C	CWSR Sheet	315	1.9	0.030	20
	CWSR Cladding [5]	350	1.5	0.059	

Note: $n = d(\ln \sigma) / d(\ln \epsilon)$ and $R' = \epsilon_{width} / \epsilon_{thickness}$ as determined in the transverse direction.

for the purpose of generating a well-defined precrack upon loading. In addition to forming the linear blister, the hydrogen charging develops a hydride particle microstructure beneath the blister; it is through this hydrided microstructure that the crack propagates during the fracture toughness determination.

In order to form a “linear” hydride blister of controlled depth with discrete hydride precipitate particles in the substrate underneath the hydride blister, the Zircaloy-4 specimen was first immersed in a solution of nitric acid (ten parts), H_2O (ten parts), and hydrofluoric acid (one part) for ~ 30 s to remove the native oxide layer. Then a gold layer was sputter-deposited on both surfaces of the specimen to act as a barrier to hydrogen diffusion into the substrate. A diamond scribe was then used to remove a thin strip of gold (~ 100 - μm wide) across the specimen width. Immediately after removal of the thin gold strip, the specimen was coated with a ≈ 20 -nm thick layer of nickel (99.995 % pure) to create a “window” for hydrogen pickup along the thin strip where the gold was removed.

The specimens were then hydrogen-charged at 370°C under a finite volume of mixture of argon and hydrogen gas (12.5 % H_2 , balance argon) at a total pressure of 6.2×10^4 Pa for times ranging from 20 to 120 min. Subsequent annealing was performed for 10 min at 400°C and then furnace cooled (see Fig. 1). The blister depths obtained ranged from ~ 50 to ~ 320 microns. Cross-sectional metallographic examinations showed that the blister depth was approximately homogeneous across the width of the sample. The average blister depth along the specimen width was determined from both cross section metallography and from the fracture surface after the test. As will be described later, the microstructure beneath the solid blister consisted of discrete hydride precipitate particles with a range of morphologies that depended on the depth of the blister.

Fracture Toughness Testing

Fracture toughness testing was performed using a four-point bend fixture such as shown in Fig. 2. This specimen configuration allowed uniform bending between the center loading pins, which were sufficiently far apart so that the stress fields resulting from the pin contact did not affect crack growth under the hydride blister. The top of the bend fixture had a V-shaped groove normal to the axial direction of the loading pins, and a 2-mm pin was placed in this groove in order to suppress any bending moment transfer to the crack induced by the contact between the upper ram and the top of the fixture.

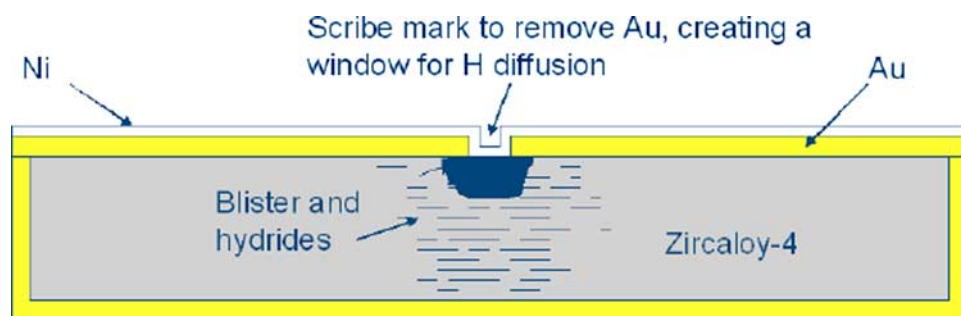


FIG. 1—Schematic representation of the specimen after hydrogen charging and annealing.

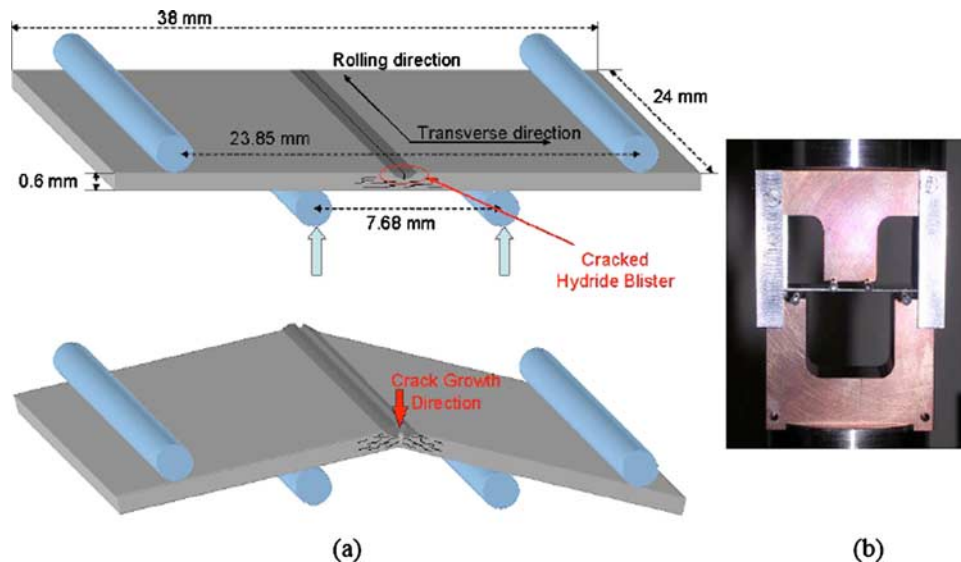


FIG. 2—(a) A schematic drawing of the four-point bend specimen, and (b) photo of the test fixture with a specimen loaded.

For the purpose of determining the initial crack length as accurately as possible, the four-point bend specimens (initially ≈ 32 mm, 38 mm in length, and ≈ 0.6 mm in thickness) were precracked by a small amount of bending. The cracking was detected using acoustic emission signals emitted from the specimen during bending. At loads less than necessary to cause yielding, blister cracking was easily identified and the crack depth was determined from two ≈ 4 -mm slices taken from each edge of the specimen. These metallographic specimens also served to characterize the hydride microstructure of each individual test specimen by etching.

Bend testing of the precracked specimen was performed in a screw-driven Instron machine with a crosshead displacement rate of 0.5 mm/min. Prior to testing the test specimens, the stiffness of the machine was measured in order to determine the elastic deformation due to the testing fixture and rams, and the machine displacement was then subtracted from the displacement measured in an actual test in order to obtain the load-line displacement corresponding to specimen response only. Given the small thickness of the sheet specimen (≈ 0.6 mm), specimen bending occurred at small loads (0.2–0.6 kN) in which case the machine load train was comparatively stiff, such that machine displacement at specimen fracture was quite small.

Upon loading, the crack growth behavior was determined in a continuous manner using the electric potential drop (EPD) technique [17]. In order to use the EPD technique, 0.275-mm diameter wires (Zirconium 702) were spot welded at fixed locations on the specimen surface using a fixture to allow for reproducible positioning of the leads. A dc power supply was used to produce a 500 mA current through the four-point bend specimen. Using ceramic pins to electrically isolate the test specimen and leads from the load frame, an amplified signal was used to monitor crack growth.

The EPD magnitude can be directly related to crack length in the bend specimens using a relationship developed by Johnson for the current specimen geometry [18]. The accuracy of Johnson's equation was verified using a series of four-point bend specimens notched at different depths using a diamond cutting wheel. Using the shallowest notch as a reference for the initial potential V_0 , Fig. 3 shows good agreement between the depth of the notch and the Johnson equation prediction. To verify the sensitivity of the method at high strain levels, the specimen with the deepest notch was heavily strained and the potential response was then measured. The potential drop response remained within experimental error of the previous undeformed value, indicating strain did not affect the potential drop measurement as long as no crack growth occurred. A second check of the accuracy of this method was performed using a cracked specimen containing a hydride blister and hydrides within the Zircaloy-4 substrate. In this case, the crack length was carefully determined by observation in a light microscope after each increment of bending and the corresponding EPD was measured, allowing for Johnson's equation to be verified, as seen in Fig. 3. Thus, Johnson's equation can be used to obtain accurate EPD crack growth measurements for our single-edge

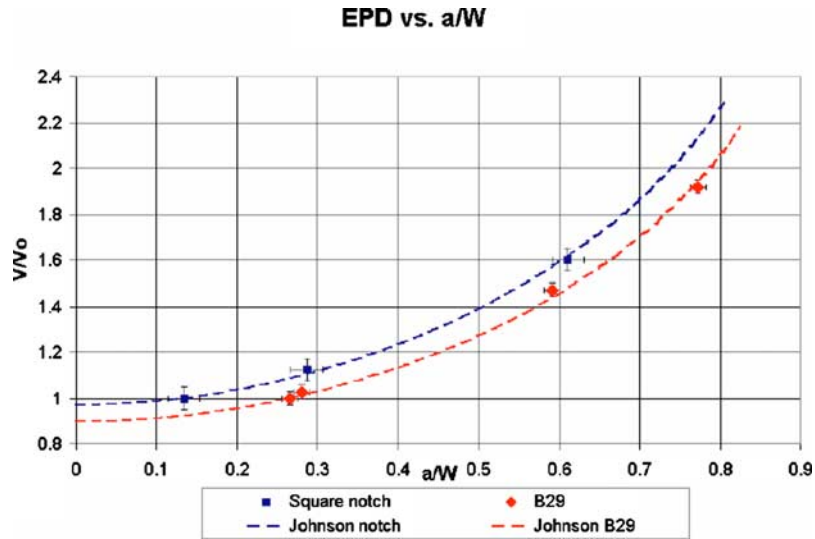


FIG. 3—Calibration curves for Johnson's equation for notched specimens and for a specimen with crack growth that was determined by sectioning (B29).

cracked four-point bend specimens if at least one (and preferably two) crack length measurement is made to benchmark the relationship. For some of the present tests, the crack lengths were determined using potential drop data and Johnson's equation based on a combination of the initial crack length (determined as described earlier) and the final crack length (measured at the end of the experiment by heat-tinting at 300°C in air).

J-Integral Analysis

Figure 4 shows a typical load-displacement response at room temperature for a specimen with a blister of a depth of approximately 115 μm . Crack growth initiation from the blister into a microstructure consisting of in-plane hydrides occurred at maximum load P_{max} only after a significant level of plasticity occurred. The large abrupt load drop that follows shortly after P_{max} was caused by $\approx 300 \mu\text{m}$ of unstable crack extension. Given the level of plastic deformation that precedes crack growth initiation such as is depicted in Fig. 4, elastic-plastic fracture mechanics were used to predict crack growth behavior. In particular, we utilized ASTM Standard E 1820 to determine the critical J-integral value at the onset of crack growth initiation during the load-displacement response [19]:

$$J_{\text{tot}} = J_{\text{el}} + J_{\text{pl}} = \frac{K_i^2 \cdot (1 - \nu^2)}{E} + J_{\text{pl}} \quad (1)$$

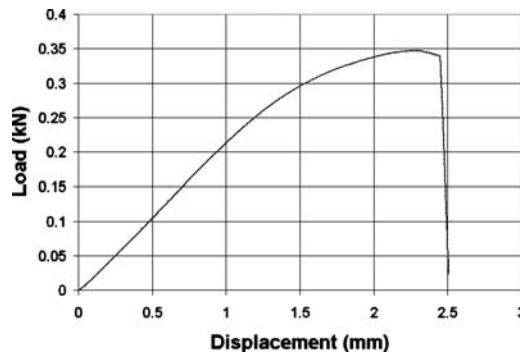


FIG. 4—The load-displacement response during four-point bending of a specimen with a 115- μm hydride blister and tested at room temperature.

$$J_{pl} = \frac{\eta \cdot A_{pl}}{B_N \cdot b_o} \quad (2)$$

where J_{el} and J_{pl} are the elastic and plastic components of J-integral, respectively; K_i is the stress intensity factor; ν is Poisson's ratio; E is Young's modulus; a_i is the crack length; B_N and W are the specimen width and thickness, respectively, for this form of cracked sheet specimen; $b_o = W - a_o$ is the initial length of the remaining ligament; A_{pl} is the amount of plastic energy spent by the applied load (the plastic energy under the load-displacement curve); and η is a geometric factor which depends on crack length.

In Eq 1, the magnitude of the elastic stress intensity factor K_i can be readily determined for our specimen geometry [20]. As seen in Eq 2, the magnitude of J_{pl} is directly dependent on the magnitude of the η parameter, and for small cracks, the η parameter is quite sensitive to the (a_i/W) value. This condition is not an issue in conventional fracture toughness testing where $a_i/W = 0.5$ (for which $\eta = 2$ and is insensitive to small changes of crack length). However, for cladding tube performance where small surface cracks may occur, it is of interest to establish the fracture toughness at small crack lengths, $a_i/W < 0.5$, which is a range where the value of η changes rapidly with crack length. Several recent studies [21–23] have used finite element modeling to calculate η for conventional four-point bend geometries which satisfy the ASTM requirements. For example, Kim's results, which were obtained for thick plate configurations, show η to depend on crack length as follows:

$$\eta = \begin{cases} 0.38 + 8.1(a/W) - 9.0(a/W)^2 & \text{for } a/W < 0.3 \\ 2 & \text{for } a/W \geq 0.3 \end{cases} \quad (3)$$

Recalling Eq 1 and assuming a plane-strain condition along the crack front, we can then obtain the K_q value for the crack growth initiation toughness from

$$K_q = \sqrt{\frac{J_{tot}E}{(1-\nu^2)}} \quad (4)$$

In the present study, the specimen geometry/test procedure and crack growth resistance often resulted in a load drop with the onset of crack growth initiation. Thus, K_q was defined on the basis of the first detectable onset of crack growth or load drop, rather than on the basis of the conventional offset load-line displacement procedure as specified in ASTM E 1820 for elastic-plastic crack growth analysis [19].

With regard to ASTM requirements for the determination of the plane-strain fracture toughness parameter K_{IC} [19], the combination of the small specimen thickness, ≈ 0.6 mm, which severely constrains the crack size and the extensive plasticity accompanying crack growth both violate the criterion for the qualification of apparent fracture toughness K_q as K_{IC} [19]. For example, if P_q is the load measured on the basis of the 95 % secant (see Fig. 4), the plasticity prior to crack growth initiation results in the ratios of $P_{max}/P_q = 1.24$ to 1.39 , or well above the $P_{max}/P_q \leq 1.10$ required K_{IC} requirement by ASTM [19]. ASTM E 1820 also places a limit on the maximum J-integral capacity for a specific specimen geometry. In the present study, the small thicknesses of the specimens do not meet the specific specimen thickness requirement for the higher observed toughness values at room temperature and all of the data at 300°C . Thus, while we associate a fracture toughness value K_q with the onset of crack growth, one must recognize the limitations of such data as possibly being specimen-size dependent. On the other hand, any determination of through-thickness crack growth of thin-wall cladding will suffer from the same limitations. Furthermore, the application of valid K_{IC} values as determined from the crack growth along thick plates is not a suitable basis for predicting failure of thin wall sheet/cladding material under through-thickness crack growth within an oriented hydride microstructure.

Results and Discussion

Hydride Microstructure

The experimental hydrogen charging procedure, which is the basis for inducing a precrack within the strip of solid hydride blister extending across the specimen width, also creates a microstructure consisting of hydride particles beneath the hydride blister. In this study, depending on blister depth, two distinct hydride microstructures were formed in the region of crack growth initiation near the hydride blister. As a result,

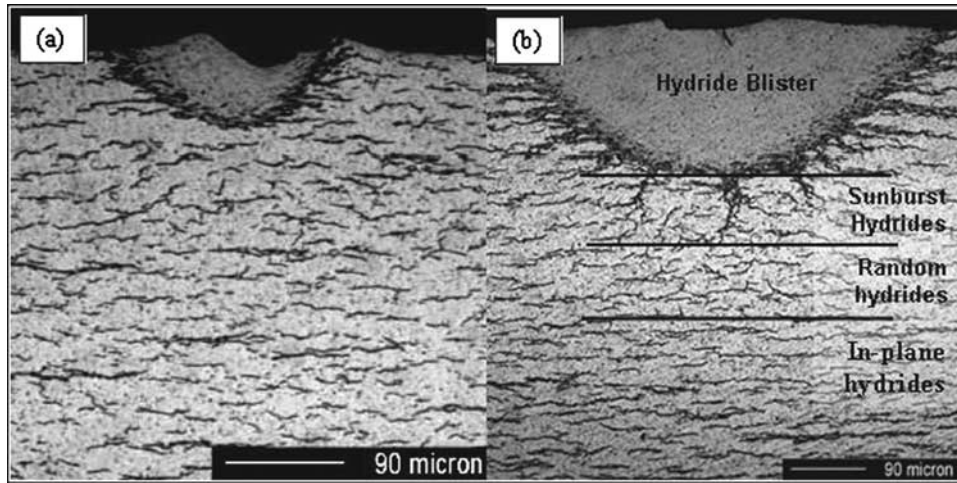


FIG. 5—Light micrographs of the cross sections of specimens with a blister depth of (a) $\sim 60 \mu\text{m}$, and (b) $\sim 210 \mu\text{m}$. Note presence of sunburst and random hydride zone beneath the deeper blister in (b).

two different fracture toughness values result at room temperature but, significantly, not at 300°C . This behavior is significant since a variety of hydride microstructures have been reported in the literature, and in certain cases, these hydrides have been shown to act as crack initiation sites and result in various forms of hydride-induced embrittlement in Zircaloy-2 and Zircaloy-4 cladding tubes [24–29].

Figure 5 illustrates the “hydride-microstructure” issue. In the region below the hydride blister, where crack growth initiation occurs, the microstructure consists of either (a) for the case of small blisters, elongated hydride particles oriented within the plane of the sheet *and* normal to the crack plane as shown in Fig. 5(a) (i.e., “in-plane” hydrides), or (b) for the case of large hydride blisters, a hydride microstructure which varies with the depth below the specimen surface in a manner shown in Fig. 5(b).

In the former case (Fig. 5(a)), crack growth initiation represents the growth of a crack on a plane roughly normal to the dominant orientation of the hydride platelets. In other words akin to through-thickness crack growth in Zircaloy cladding tubing containing “circumferential” hydrides, the crack intersects the broad faces of the hydride platelets. As detailed by the microstructural characterization of each individual test specimen, crack growth initiation within specimens with small hydride blisters (i.e., small precracks less than about $120\text{-}\mu\text{m}$ deep) occurred by the growth of a crack into a comparatively uniform microstructure consisting of in-plane hydrides with faces that are oriented 90° to the crack growth direction.

In contrast, test specimens containing large hydride blisters, such as depicted in Fig. 5(b), exhibit three distinct forms of hydrides present within the Zircaloy substrate beneath the blister. Figure 5(b) shows that, in addition to the solid hydride blister whose depth is roughly one-half of its width, the microstructures beneath blisters that are more than about $140\text{-}\mu\text{m}$ deep consist of the following:

1. Sunburst Hydrides: Emanating radially from the hydride blister are “sunburst hydrides.” Above a threshold blister depth of $\approx 140 \mu\text{m}$, the sunburst hydride depth (Y_s) increases with increasing blister depth (X_b) in a manner expressed approximately by $(dY_s/dX_b) \approx 0.4X_b$.
2. Mixed Hydride Zone: Adjacent to the sunburst hydrides, there is a transition zone which contains discrete hydride particles of different orientations. A significant fraction ($\geq 1/3$) of the hydride platelets have their normal oriented parallel to the sample surface, so that the platelet surfaces are parallel to the crack plane *and* crack growth direction (i.e., these are akin to radial hydrides within a cladding tube). These out-of-plane hydrides are mixed with in-plane hydrides and a few hydrides that are oriented at about 45° to both the in-plane and out-of-plane hydrides. For large blisters ($\geq \approx 140 \mu\text{m}$, the depth of the mixed hydride zone (Y_r) also increases with increasing blister depth (X_b) in a manner expressed approximately by $(dY_r/dX_b) \approx 0.5X_b$.
3. In-Plane Hydride Zone: Finally, the remainder of the Zircaloy sheet contains discrete hydride platelets that are parallel to the sample surface and thus perpendicular to the crack growth direction *and* the crack plane (in-plane hydrides), as seen throughout the thickness in samples containing thinner blisters (see Fig. 5(a)). These hydrides are akin to the “circumferential hydrides,” typically observed in Zircaloy cladding tubes.

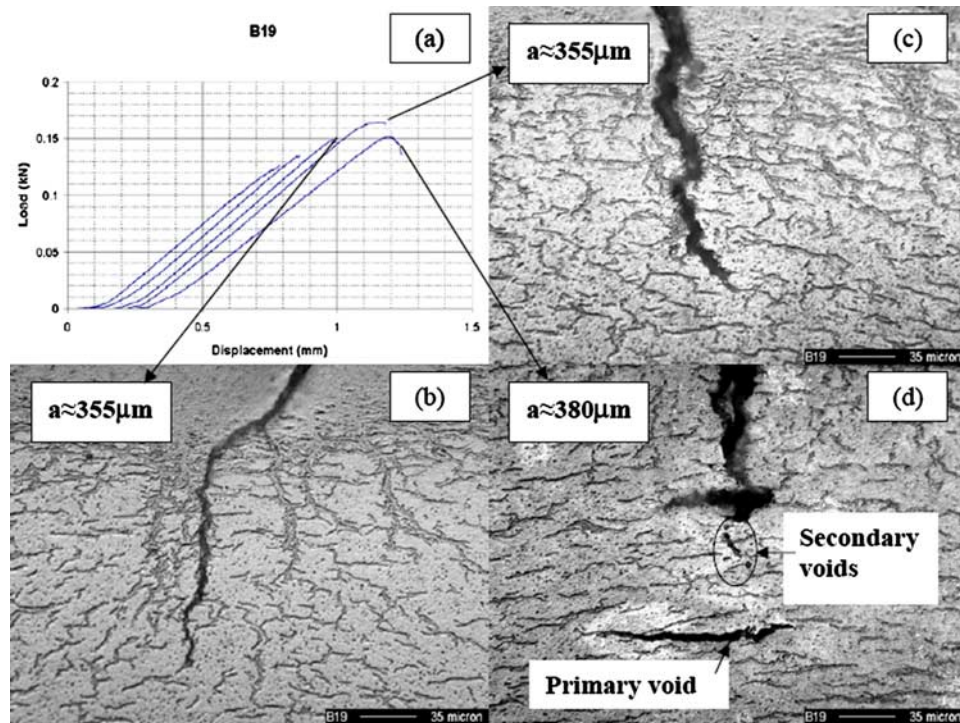


FIG. 6—The evolution of the crack profile with increased bending during the interrupted testing of a specimen with a $\approx 215\text{-}\mu\text{m}$ blister. Test was performed at room temperature.

While the hydride microstructures were relatively uniform across the *width* of the blister (see Fig. 5), the small volume of sheet material that was charged with hydrogen made it impossible to use chemical means to determine the actual hydrogen contents of the Zircaloy directly beneath the blister through which crack propagation occurs. To assess the hydrogen contents of the samples tested, the density of *in-plane* hydrides was measured for each individual test specimen by using the line intercept method to determine the inter-particle spacing along a line normal to the sheet surface and located beneath the hydride blister. Those results indicate an average spacing of all in-plane hydrides in the range of $\approx 15\text{--}25 \mu\text{m}$, which was relatively independent of depth within a specimen, suggesting relatively uniform hydrogen content throughout the remaining thickness of the sheet. No significant trend was observed between the average spacing of the in-plane hydrides and blister depth, suggesting no gross differences in substrate hydrogen content with blister depth.

Within the in-plane hydride region in the substrate, two distinct size groups of the particles were apparent. There were many small hydride particles in the range of $0.4\text{-}\mu\text{m}$ thick and with lengths in the $20\text{--}50 \mu\text{m}$ range (as measured on the specimen surface using backscatter imaging in the scanning electron microscope); these particles dominated the inter-particle spacing of $\approx 20 \mu\text{m}$ described above. There was also a second size group consisting of a small population of much larger hydride particles with (surface) lengths in the $100\text{--}200\text{-}\mu\text{m}$ range and with thicknesses $\approx 0.7 \mu\text{m}$. These larger hydride particles, which resulted from the annealing at 400°C followed by a furnace cool, had inter-particle spacings of about $\sim 60\text{--}80 \mu\text{m}$. In a later section, an examination of the fracture surfaces will show that the small population of large hydrides form the primary voids that are integral to the Mode I crack growth process at room temperature.

Crack Growth, Hydride Microstructure, and Fracture Toughness

The solid hydride blister is known to be brittle at temperatures at least to 400°C [30]. Accordingly, for both hydride blister depths illustrated in Fig. 5, examinations of bend specimens after initial loading showed that the brittle hydride blister cracked prior to any large-scale plastic deformation of the substrate. Occasionally, more than one long precrack would form, invalidating the test and its results, which were not considered in our analysis. Once the blister cracks, the subsequent crack growth behavior depends on test temperature and the character of the substrate hydride microstructure, as shown in Figs. 6 and 7.

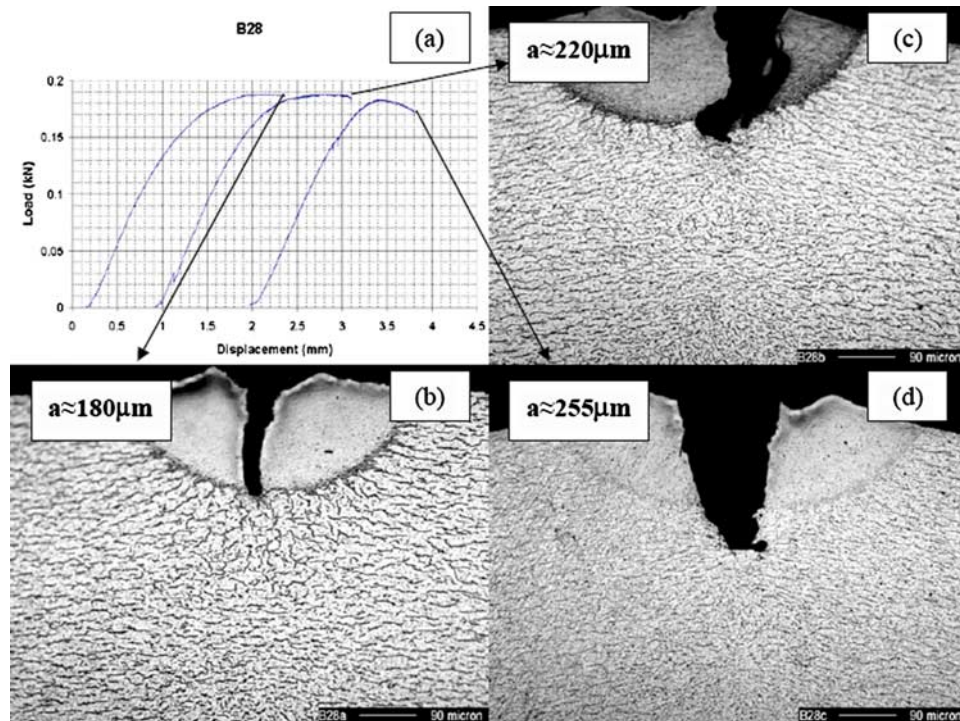


FIG. 7—The evolution of the crack profile with increased bending during the interrupted testing of a specimen with a $\approx 175\text{-}\mu\text{m}$ blister. Test was performed at 300°C .

In the case of the specimens with small blisters tested at room temperature and for the specimens precracked *and* tested at 300°C , the precrack arrested at the blister-substrate interface as shown in Fig. 5(a). In those cases, subsequent testing resulted in a load-displacement response that showed a smooth transition to plastic bending with the load increasing to a maximum load value and then continuously decreasing such as in Fig. 4 (at room temperature) or Fig. 7(a) (at 300°C). In such cases, the onset of crack growth was detected by an acceleration of load loss and confirmed by potential drop data. As shown in Fig. 5(a) for specimens with small blisters, crack growth proceeded into an *in-plane* hydride microstructure. Thus, the resulting crack growth initiation toughness K_q is that for through-thickness crack growth initiation into an in-plane hydride microstructure similar to that in Fig. 5(a) or to that in the lower section of Fig. 5(b).

For specimens with deep blisters such as that illustrated in Fig. 5(b), the precracking process at room temperature created a single crack that propagated not only through the blister *but also* well into the adjoining sunburst hydride field, as shown in Fig. 6(b). Examinations of the load-displacement responses of several specimens showed that crack growth through the sunburst hydrides occurred in the *absence* of any discernible load drop. Thus, in these cases, the initial crack length upon subsequent loading was the sum of the blister depth plus the length of sunburst hydride in the plane of the crack. As a result of this particular precracking behavior, Fig. 6(b) shows that the first (small) load drop (Fig. 6(b)) is associated with a crack that has already propagated from the sunburst hydrides through the field of mixed hydrides and arrested in a region where in-plane hydrides began to dominate the microstructure. Subsequent loading (Fig. 6(c)) results in large-scale yielding (specimen is plastically bent) and is characterized by crack arrest and significant crack-tip deflection. Crack growth into the in-plane hydride field is difficult, as it requires significant plastic deformation of the specimen (Fig. 6(d)) to cause a small degree of crack growth ($\approx 25\ \mu\text{m}$). Figure 6(d) shows that at this point in the bending process the crack tip is quite blunted (indeed in Fig. 6(d), crack-tip branching has occurred) with large primary voids forming along the plane normal to the crack plane following elongated hydrides ahead of the crack tip.

Taken as a whole, the above behavior clearly indicates that at room temperature the crack growth resistance is sensitive to the hydride microstructure. Specifically, the precrack growth through both the hydride blister *and* the sunburst hydrides suggests the ease of crack growth when the crack plane and crack growth direction coincides with the orientation of the hydride platelets, providing a continuity of crack path. These results also indicate that through-thickness crack growth initiation through microstructure

TABLE 3—A listing of fracture toughness values for through-thickness crack growth initiation in individual tests as a function of the hydride microstructure.

Temperature	Fracture Toughness K_q	Hydride Microstructure
25°C	23, 27, and 28 MPa√m	Random/mixed hydrides with platelet orientations both in-plane and out-of-plane of sheet.
25°C	66 and 80 MPa√m	Predominantly in-plane hydrides with significant presence of large particles that cause crack-tip branching.
300°C	78, 82, and 88 MPa√m	Crack blunting at blister-matrix interface occurs even when sunburst hydrides should still be present.

containing a mixture of in-plane and out-of-plane hydrides is significantly easier than that for crack growth through large in-plane hydrides where crack branching and deflection occurs. Thus, as discussed by Bertolino et al. [11,12], fracture toughness is expected to be quite sensitive to hydride platelet orientation at room temperature.

That the fracture toughness is sensitive to hydride platelet microstructure is consistent with fracture models such as the Rice-Johnson model which assumes crack growth initiation can occur if the length scale of the heavily stretched region (λ) within the plastic zone is of the order of the ligament between cracked particles [31]. Used with some success to relate fracture toughness to microstructure in Al-base alloys in particular (see, for example, Ref. [32]), this analysis estimates the magnitude of stretch region λ is related to the fracture toughness as

$$\lambda \approx 0.5 \frac{K_q^2}{E\sigma_y} \quad (5)$$

where σ_y is the yield stress, and E is Young's modulus.

In the present case, Eq 5 should provide a very crude estimate of the scale of the ligament between cracked hydride particles within the Zircaloy matrix at the onset of crack growth at room temperature. For the case of the mixed hydrides where $K_Q \cong 25$ MPa√m, $\lambda \approx 5$ μm, which is roughly similar to the spacing between the mixed hydride particles (see Fig. 5(b)). In contrast, for crack growth initiation into an in-plane hydride field where the large hydrides (and therefore the primary void initiation sites) are roughly 60–80 μm apart, the observed K_Q value of $\cong 75$ MPa√m, yields $\lambda \approx 50$ μm, which is on the scale of the inter-particle spacing between the large in-plane hydrides. As will be shown in the fractography section to follow, the large in-plane hydrides serve as the primary void sites for fracture at room temperature. Although only approximate, the above analysis is consistent with the observation that fracture toughness is sensitive to hydride microstructure.

Compared to the crack growth behavior for deep blisters at room temperature, Fig. 7 shows a much different load-displacement and crack growth process in a test conducted at 300°C. Even though this specimen contained extensive sunburst hydrides prior to the test at room temperature, crack growth at 300°C is arrested near the blister-matrix interface despite general yielding of the specimen; see Figs. 7(a) and 7(b). The significant plastic deformation prior to the first unload of this test results in only minimal crack growth (≈ 5 μm) and extensive crack-tip blunting near the blister-substrate interface. Further crack growth (Figs. 7(c) and 7(d)) occurs only after much more plastic deformation, by which time the specimen shows a distinctly bent profile. This is evidence of a high level of crack growth resistance at 300°C as also manifested by extensive crack-blunting. It is noteworthy that the crack in Fig. 7(d) almost has the profile of a blunt notch. This crack geometry is remindful of the crack-tip geometry from which mixed Mode I +II crack growth inclined on a plane roughly 45° to the specimen surface has been previously observed in hydrided Zircaloy-4 [4].

As shown in Table 3, the fracture toughness behavior is qualitatively consistent with the crack growth observations described above. Crack growth at room temperature through the field of mixed-orientation hydrides is characterized by a comparatively low fracture toughness, $K_q \approx 25$ MPa√m. The lower fracture resistance is likely a reflection of the presence of significant amounts of out-of-plane hydrides in this

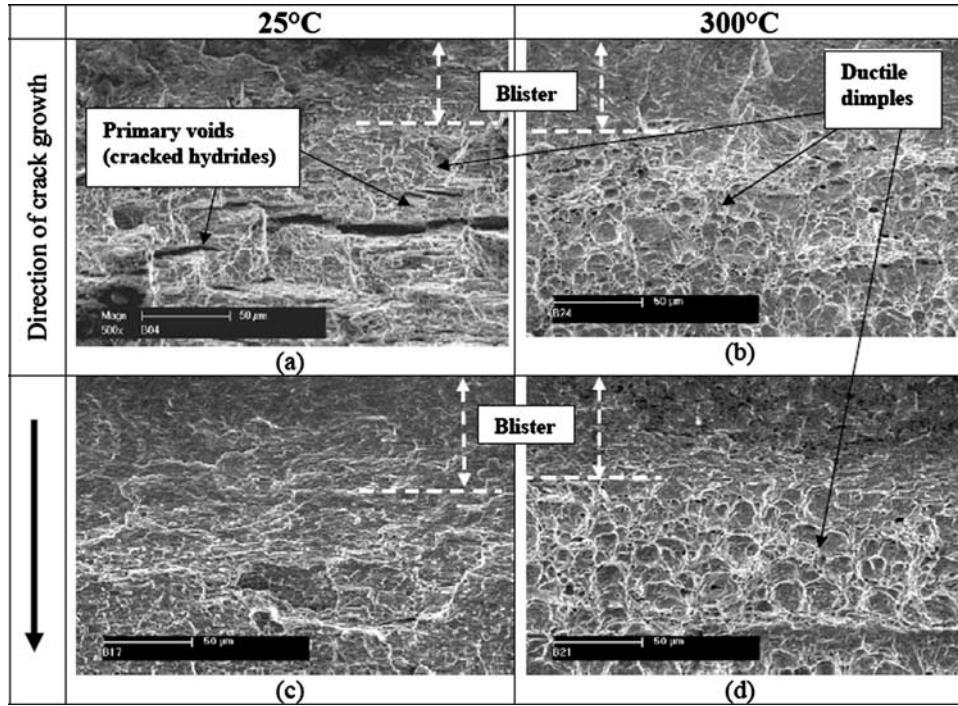


FIG. 8—Secondary electron SEM images of the fracture surfaces showing the region directly below the blister for a $\sim 100\text{-}\mu\text{m}$ blister specimen fractured at 25°C (a), and 300°C (b), and for a $\sim 200\text{-}\mu\text{m}$ blister specimen fractured at 25°C (c), and 300°C (d).

mixed hydride field. We would expect that a low K_q value in this case is promoted by cleavage or matrix-particle decohesion (which seems to be the case based on our initial fractography) along the faces of the hydride platelets aligned with the crack growth direction.

In contrast to the above behavior, K_q is much higher, ($K_q \cong 75 \text{ MPa}\sqrt{\text{m}}$), when the hydrides are oriented predominantly in the plane of the sheet and (importantly) normal to both the crack plane and the crack growth direction. In this case, despite the presence of elongated hydride particles that initiate large primary voids, their presence also causes crack-tip deflection and crack branching (see Fig. 6(d)). The net effect is a K_q value ($75 \text{ MPa}\sqrt{\text{m}}$) that is close to $K_q \cong 85 \text{ MPa}\sqrt{\text{m}}$ for *unhydrided* CWSR Zircaloy-4 cladding tube as determined by Bertsch and Hoffelner for axial crack growth [33]. Thus, these results suggest that in-plane hydrides have only a minor net effect on through-thickness crack growth, at least at concentrations in the range of the present study.

At 300°C , the hydride particles within the matrix resist fracture and do not appear to participate in the crack growth process (Fig. 7). In short, as observed by Grigoriev for crack growth along the axes of hydrided Zircaloy-2 cladding tubes [13], there appears to be no effect of hydrogen on the fracture toughness at 300°C . In the present case, the fracture toughness value of $K_q \cong 78 \text{ MPa}\sqrt{\text{m}}$ (Table 3) is significantly less than that observed by Grigoriev ($K_q \cong 105 \text{ MPa}\sqrt{\text{m}}$) also at 300°C . This difference in toughness levels seems reasonable given the comparatively large amount of through-thickness deformation (and low level of stress triaxiality) that should accompany the mixed Mode I+III crack growth along the axis of the thin cladding tube wall in Grigoriev's tests. Nevertheless, given the much smaller flow stress of the Zircaloy-4 at this temperature (see Table 2), the relatively high K_q value ($K_q \cong 78 \text{ MPa}\sqrt{\text{m}}$) is characterized by a comparatively large plastic displacement component necessary to induce crack growth. Thus, except for deep cracks, crack growth at 300°C will be accompanied by considerable plastic strain.

Fracture Surface Behavior

Consistent with the crack growth behavior as viewed from specimen cross sections (Figs. 8 and 9), the fracture surfaces of specimens with large hydride blisters show distinct changes in appearance as the crack propagates. For example, Fig. 8(c) shows that the room temperature fracture surface immediately beneath a comparatively large blister is relatively flat and characterized by shallow dimples and tear ridges. Such a fracture surface is consistent with a low energy fracture process as the crack propagates through both

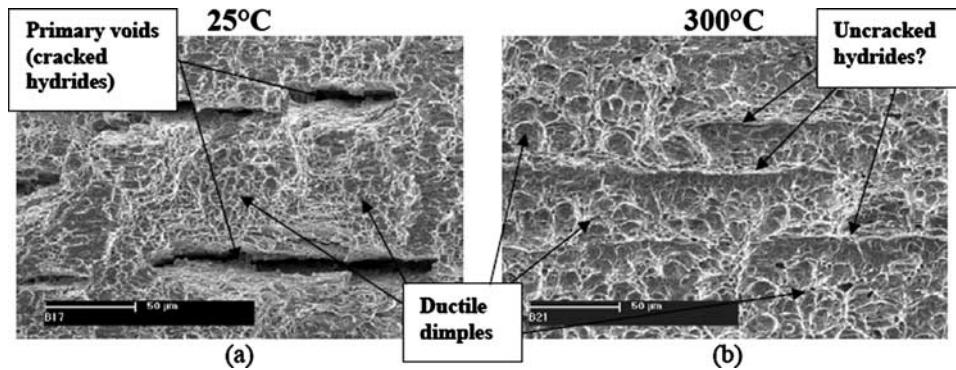


FIG. 9—Secondary electron SEM images showing (a) a large cracked hydride surrounded by ductile dimples in a specimen tested at 25°C, and (b) uncracked hydrides and ductile dimples in a specimen tested at 300°C. Both images are located ~200 μm under a ~200-μm blister.

sunburst hydrides and a mixed hydride particle field containing a significant density of out-of-plane hydrides that create cleavage or void facets co-planar with the growing crack. The result is a comparatively low fracture toughness, $K_q \approx 20$'s $\text{MPa}\sqrt{\text{m}}$.

At depths sufficiently far beneath the hydride blister such that the crack propagates into the region of *in-plane* hydrides, large primary voids elongated in an orientation normal to the crack plane *and* growth direction are readily evident on the fracture surface formed at room temperature; see Fig. 8(a). These large voids ($>100 \mu\text{m}$ in length) have an average spacing of $\sim 60\text{--}80 \mu\text{m}$ and correspond to the larger hydrides seen in metallographic observations of the Zircaloy-4 matrix (Fig. 5(b)). As discussed previously, the presence of large elongated in-plane hydrides cause crack deflection/branching, thus increasing the crack growth resistance ($K_q \approx 70$'s $\text{MPa}\sqrt{\text{m}}$) relative to that observed in the mixed hydride region ($K_q \approx 20$'s $\text{MPa}\sqrt{\text{m}}$). Although not reported here, a positive tearing modulus results as the crack grows into the in-plane hydride region.

The fracture surface formed at 300°C is distinctly different from that formed at room temperature. For example, at the depth directly beneath the blister but at 300°C, Fig. 8(d) shows well developed dimples characteristic of microvoid coalescence during ductile fracture. The dimples in Fig. 8(d), which are somewhat elongated due to the tendency toward an inclined mixed Mode I/II fracture plane, are much deeper than the “room temperature” tear ridges in Fig. 8(c); the resulting 300°C toughness, $K_q \approx 75 \text{MPa}\sqrt{\text{m}}$, is also much higher than the room temperature value of $K_q \approx 20$'s $\text{MPa}\sqrt{\text{m}}$ for a somewhat similar microstructure of mixed hydrides (assuming that these hydrides have not all dissolved upon temperature increase).

Figure 9 shows a comparison of the fracture surfaces in a microstructural region that should contain in-plane hydride platelets after fracture at 25°C (Fig. 9(a)) as compared to that after 300°C fracture (Fig. 9(b)). Examinations of many regions of fracture surfaces formed at 300°C show *no* evidence that the hydrides initiate the failure process or participate directly in fracture at this temperature. As shown in Fig. 9(b), the 300°C fracture surfaces well beneath the blister are consistently characterized by microvoid dimples separating elongated tear ridges whose orientation and spacing is consistent with the large elongated hydrides that form the primary voids at room temperature (Fig. 9(a)). Furthermore, their appearance at 300°C as *elevated* tear ridges on the fracture surface suggests that, if indeed these are the elongated hydrides, they not only do not crack, but instead, they appear to fail by plastic thinning with significant ductility. (It is likely that the hydrides are thinner at 300°C due to some hydrogen being redissolved into the Zr matrix.)

Conclusions

1. An experimental procedure has been developed to determine the fracture toughness of hydrided CWSR Zircaloy-4 sheet under *through-thickness* crack growth conditions. The procedure relies on four-point bending of specimens that contain a narrow strip of brittle hydride blister across their width. The blister forms a precrack upon initial loading such that the subsequent crack growth initiation conditions can be determined using elastic-plastic fracture mechanics analysis.

2. At room temperature, the crack growth behavior and fracture toughness is sensitive to the microstructure of the hydride particles beneath the solid hydride blister. For through-thickness crack growth within a mixed microstructure of in-plane and out-of-plane hydrides, $K_q \approx 25 \text{ MPa}\sqrt{\text{m}}$. In this case, the presence of significant levels of out-of-plane hydride platelets (akin to radial hydrides in cladding tubes) contribute to the comparatively low fracture toughness as they align with the through-thickness crack growth. *In contrast*, preliminary results indicate that K_q is much higher, $K_q \approx 75 \text{ MPa}\sqrt{\text{m}}$, when the crack grows through a zone of in-plane hydride platelets oriented predominantly within the plane of the sheet (akin to circumferential hydrides in cladding tubes). The resulting interaction between the crack and hydride platelets that are oriented normal to both the crack plane and crack growth direction cause crack deflection and branching.
3. At 300°C, initial data indicate $K_q \approx 83 \text{ MPa}\sqrt{\text{m}}$. Despite the similarity of this K_q value to that for in-plane crack growth at room temperature, the fracture surfaces formed at 300°C suggest little direct involvement of hydrides in the crack growth process, in contrast to their dominant role at room temperature. Furthermore, the comparatively low flow stress at 300°C gives rise to an elastic-plastic response and a fracture strain that is significantly higher than at room temperature for similar crack lengths.

Acknowledgments

The authors gratefully acknowledge the financial support and encouragement from Ralph Meyer and Harold Scott at the Nuclear Regulatory Commission. Surface preparation prior to hydrogen charging was performed at the Penn State Nanofabrication facility. The authors also acknowledge helpful discussions with Christophe Poussard and Claude Sainte-Catherine of the CEA, as well as Jean Desquines at IRSN.

References

- [1] Bai, J. B., Prioul, C., and Francois, D., "Hydride Embrittlement in Zircaloy-4 Plate: Part Influence of Microstructure on the Hydride Embrittlement in Zircaloy-4 at 20 C and 350 C," *Metall. Mater. Trans. A*, Vol. 25A, 1994, pp. 1185–1197.
- [2] Meyer, R. O., McCardell, R. K., Chung, H. M., Diamond, D. J., and Scott, H. H., "A Regulatory Assessment of Test Data for Reactivity Initiated Accidents," *Nuclear Safety*, Vol. 37, 1996, pp. 271–288.
- [3] Garde, A. M., Smith, G. P., and Pirek, R. C., "Effects of Hydride Precipitate Localization and Neutron Fluence on the Ductility of Irradiated Zircaloy-4," *11th International Symposium on Zr in the Nuclear Industry*, ASTM STP 1295, Garmisch-Partenkirchen, Germany, ASTM International, West Conshohocken, PA, 1996, pp. 407–430.
- [4] Glendening, A., Koss, D. A., Pierron, O. N., Motta, A. T., and Daum, R. S., "Failure of Hydrided Zircaloy-4 Under Equal-Biaxial and Plane-Strain Tensile Deformation," *J. ASTM Int.*, Vol. 2, 2005, pp. 833–848.
- [5] Link, T. M., Koss, D. A., and Motta, A. T., "Failure of Zircaloy Cladding Under Transverse Plane-Strain Deformation," *Nucl. Eng. Des.*, Vol. 186, 1998, pp. 379–394.
- [6] Daum, R. S., Majumdar, S., Tsai, H. C., Billone, M. C., Bates, D. W., Koss, D. A., and Motta, A. T., "Embrittlement of Hydrided Zircaloy-4 Under RIA-Like Conditions," *13th ASTM International Symposium on Zr in the Nuclear Industry*, ASTM STP 1423, Annecy, France, ASTM International, West Conshohocken, PA, 2001, pp. 702–719.
- [7] Huang, F. H., "Brittle Fracture Potential of Irradiated Zircaloy-2 Pressure Tubes," *J. Nucl. Mater.*, Vol. 207, 1993, pp. 103–115.
- [8] Kreyns, P. H., Bourgeois, W. F., White, C. J., Charpentier, P. L., Kammenzind, B. F., and Franklin, D. G., "Embrittlement of Reactor Core Materials," *Proceedings of the 1995 11th International Symposium on Zirconium in the Nuclear Industry*, 11–14 Sept. 1995, Garmisch-Partenkirchen, Germany, ASTM International, West Conshohocken, PA, 1996, pp. 758–781.
- [9] Chow, C. K. and Simpson, L. A., "Analysis of the Unstable Fracture of a Reactor Pressure Tube Using Fracture Toughness Mapping," *Case Histories Involving Fatigue and Fracture Mechanics*, Charleston, SC, ASTM International, West Conshohocken, PA, 1986, pp. 78–101.

- [10] Davies, P. H. and Stearns, C. P., "Fracture Toughness Testing of Zircaloy-2 Pressure Tube Material with Radial Hydrides Using Direct Current Potential Drop," *Fracture Mechanics: 17th Volume, 17th National Symposium on Fracture Mechanics*, Albany, NY, ASTM International, West Conshohocken, PA, 1986, pp. 379–400.
- [11] Bertolino, G., Meyer, G., and Perez Ipina, J., "Effects of Hydrogen Content and Temperature on Fracture Toughness of Zircaloy-4," *J. Nucl. Mater.*, Vol. 320, 2003, pp. 272–279.
- [12] Bertolino, G., Perez Ipina, J., and Meyer, G., "Influence of the Crack-Tip Hydride Concentration on the Fracture Toughness of Zircaloy-4," *J. Nucl. Mater.*, Vol. 348, 2006, pp. 205–212.
- [13] Grigoriev, V., Josefsson, B., and Rosborg, B., "Fracture Toughness of Zircaloy Cladding Tubes," *11th ASTM International Symposium on Zr in the Nuclear Industry*, ASTM STP 1295, Garmisch-Partenkirchen, Germany, ASTM International, West Conshohocken, PA, 1996, pp. 431–447.
- [14] Kearns, J. J. and Woods, C. R., "Effect of Texture, Grain Size and Cold Work on the Precipitation of Oriented Hydrides in Zircaloy Tubing and Plate," *J. Nucl. Mater.*, Vol. 20, 1966, p. 241.
- [15] Delobelle, P., Robinet, P., Bouffieux, P., Greyer, P., and LePichon, I., "A Unified Model to Describe the Anisotropic Viscoplastic Zircaloy-4 Cladding Tubes," *11th International Symposium on Zr in the Nuclear Industry*, ASTM STP 1295, Garmisch-Partenkirchen, Germany, ASTM International, West Conshohocken, PA, 1996, pp. 373–393.
- [16] Nakatsuka, M., "Mechanical Properties of Neutron Irradiated Fuel Cladding Tube," *J. Nucl. Sci. Technol.*, Vol. 28, 1991, pp. 356–368.
- [17] Saxena, A. and Muhlstein, C. L., "Crack Length Measurement," *Mechanical Testing and Evaluation*, ASM International, Materials Park, OH, 2000, pp. 174–178.
- [18] Johnson, H. H., "Calibrating the Electric Potential Method for Studying Slow Crack Growth," *Mater. Res. Stand.*, Vol. 5, 1965, pp. 442–445.
- [19] ASTM Standard Practice E 1820-06, "Standard Test Method for Measurement of Fracture Toughness," *Annual Book of ASTM Standards*, ASTM International, West Conshohocken, PA, 2006.
- [20] Anderson, T. L., *Fracture Mechanics Fundamentals and Applications*, Taylor and Francis/CRC Press, Boca Raton, FL, 2005.
- [21] Kim, Y. J., "Plastic Eta Factors Based on Load-CMOD Records for SE(B) Toughness Testing Specimens," *Key Eng. Mater.*, Vol. 183–187, 2000, pp. 133–138.
- [22] Kim, Y. J., "Experimental J Estimation Equations for Single-Edge Cracked Bars in Four-Point Bend: Homogeneous and Bi-Material Specimens," *Eng. Fract. Mech.*, Vol. 69, 2002, p. 793.
- [23] Kirk, M. T. and Dodds, R. H., "J and CTOD Estimation Equations for Shallow Cracks in Single Edge Notch and Bend Specimens," *J. Test. Eval.*, Vol. 21, 1993, pp. 228–238.
- [24] Edsinger, K., Davies, J. H., and Adamson, R. B., "Degraded Fuel Cladding Fractography and Fracture Behavior," *Zirconium in the Nuclear Industry: 12th International Symposium*, ASTM STP 1354, G. P. Sabol and G. D. Moan, Eds., ASTM International, West Conshohocken, PA, 2000 pp. 316–339.
- [25] Armijo, J. S., "Performance of Failed Fuel," *Proceedings of 1994 International Topical Meeting on LWR Fuel Performance*, April 1994, American Nuclear Society, West Palm Beach, FL, 1994, pp. 410–422.
- [26] Lin, K.-F., Chung, C.-S., Yeh, J.-J., Chen, J.-H., Chu, S.-S., and Lin, L.-F., "Investigation on the Post-Defect Deterioration of Nonbarrier BWR Failed Rods," *Proceedings of 1994 International Topical Meeting on LWR Fuel Performance*, April 1994, American Nuclear Society, West Palm Beach, FL, 1994 pp. 377–390.
- [27] Cheng, B., Oberlander, B. C., Wiesenack, W., Yagnik, S., and Turnbull, J., "An In-Reactor Simulation Test to Evaluate Root cause of Secondary Degradation of Defective BWR Fuel Rod," *Zirconium in the Nuclear Industry: 13th International Symposium*, ASTM STP 1423, G. D. Moan and P. Rudling, Eds., ASTM International, West Conshohocken, PA, 2002, pp. 616–633.
- [28] Yang, R. L., "Resolving our Understanding of REP-Nal Microstructural Analysis," *Proceedings of the 2004 International Meeting on LWR Fuel Performance*, Orlando, FL, 19–22 Sept. 2004, Paper No. 1094, 2004, pp. 565–575.
- [29] Hayashi, H., Etoh, Y., Tsukuda, Y., Shimada, S., and Sakurai, H., "Outside-In Failure of BWR Segment Rods During Power Ramp Tests, Fuel Failure in Water Reactors: Causes and Mitigation," *Proceedings of a Technical Meeting held in Bratislava, Slovakia*, 17–21 June 2002, IAEA-

TECDOC-1345, 2003 pp. 148–163.

- [30] Pierron, O. N., Koss, D. A., Motta, A. T., and Chan, K. S., “The Influence of Hydride Blisters on Fracture of Zircaloy 4,” *J. Nucl. Mater.*, Vol. 322, 2003, pp. 21–35.
- [31] Rice, J. R. and Johnson, M. A., “The Role of Crack-Tip Geometry Changes in Plane Strain Fracture,” *Inelastic Behavior of Solids*, McGraw-Hill, New York, NY, 1970, pp. 641–672.
- [32] Garrison, W. M. and Moody, N. R., “Ductile Fracture,” *J. Phys. Chem. Solids*, Vol. 48, 1987, pp. 1035–1074.
- [33] Bertsch, J. and Hoffelner, W., “Crack Resistance Curves Determination of Tube Cladding Material,” *J. Nucl. Mater.*, Vol. 352, 2006, pp. 116–125.